

DOCUMENT CONTROL SHEET

	ORIGINATOR'S REF. NLR-TP-2003-100	SECURITY CLASS. Unclassified				
ORIGINATOR National Aerospace Laboratory NLR, Amsterdam, The Netherlands						
TITLE Towards affordable CFD simulations of rotors in forward flight A feasibility study with future application to vibrational analysis						
PREPARED FOR: Presentation at the 59 th American Helicopter Society Forum, Phoenix, Arizona, USA, 6-8 May 2003						
AUTHORS H. van der Ven and O.J. Boelens	DATE February 2003	<table border="1" style="width: 100%; border-collapse: collapse;"> <tr> <td style="width: 50%;">pp</td> <td style="width: 50%;">ref</td> </tr> <tr> <td style="text-align: center;">31</td> <td style="text-align: center;">20</td> </tr> </table>	pp	ref	31	20
pp	ref					
31	20					
DESCRIPTORS						
ABSTRACT <p>In this report a new solution method for the simulation of rotors in forward flight is presented. The novelty of the solution method is that it turns a dynamic problem into a static problem. The solution method will render the quantitative vibrational analysis of helicopters feasible and affordable.</p> <p>For the vibrational analysis of the rotor/hub/pylon system of a helicopter it is essential that</p> <ul style="list-style-type: none"> • the aerodynamics model is <i>strongly</i> coupled to the elasto-mechanical models, • the aerodynamics model is based on first principles, • the rotor system is trimmed on the basis of the CFD results. <p>Straightforward implementation of these points of departure would yield a helicopter vibrations analysis system which requires prohibitively large computing times, due to disparate time scales and high resolution requirements. The new solution method decreases both the numerical complexity of the coupled system, and its computational complexity. Local grid refinement can be used to decrease the CFD grid size, without jeopardising the parallel efficiency of the method.</p> <p>The new solution method is applied to the simulation of the flow around a rotor in forward flight, combined with local grid refinement in both space and time. The method demonstrates good vortex capturing capabilities on a space-time grid which is a factor 15 smaller than the equivalent spatial grid of conventional simulations.</p>						



NLR-TP-2003-100

Towards affordable CFD simulations of rotors in forward flight

A feasibility study with future application to vibrational analysis

H. van der Ven and O.J. Boelens

Prepared for presentation at the 59th American Helicopter Society Forum, Phoenix, Arizona, USA, 6-8 May 2003.

The contents of this report may be cited on condition that full credit is given to NLR and the authors.

Working Plan number: A.1.B.4




Owner: National Aerospace Laboratory NLR

Division: Fluid Dynamics

Distribution: Unlimited

Classification title: Unclassified

February 2003

Approved by author:  2001/3/5	Approved by project manager:  5/3/2003	Approved by project managing department:  5/3/2003
--	---	---

Summary

In this report a new solution method for the simulation of rotors in forward flight is presented. The novelty of the solution method is that it turns a dynamic problem into a static problem. The solution method will render the quantitative vibrational analysis of helicopters feasible and affordable.

For the vibrational analysis of the rotor/hub/pylon system of a helicopter it is essential that

- the aerodynamics model is *strongly* coupled to the elasto-mechanical models,
- the aerodynamics model is based on first principles,
- the rotor system is trimmed on the basis of the CFD results.

Straightforward implementation of these points of departure would yield a helicopter vibrations analysis system which requires prohibitively large computing times, due to disparate time scales and high resolution requirements. The new solution method decreases both the numerical complexity of the coupled system, and its computational complexity. Local grid refinement can be used to decrease the CFD grid size, without jeopardising the parallel efficiency of the method.

The new solution method is applied to the simulation of the flow around a rotor in forward flight, combined with local grid refinement in both space and time. The method demonstrates good vortex capturing capabilities on a space-time grid which is a factor 15 smaller than the equivalent spatial grid of conventional simulations.



Contents

Abbreviations	5
Symbols	6
1 Introduction	7
1.1 Aeroelastic response problems	7
1.2 Outline	8
2 Multitime multigrid algorithm	10
2.1 Basic idea	10
2.2 Benefits	10
3 Rotorcraft simulation	12
3.1 Operational Loads Survey helicopter rotor simulation	12
3.2 Space-Time grid adaptation	12
3.3 Results	13
3.4 Computational characteristics	14
3.5 Discussion of computational complexity	15
3.6 Grid size estimates	17
4 Conclusions	19
5 References	20

1 Table

12 Figures

(31 pages in total)



Abbreviations

BVI	Blade-Vortex Interaction
CAMRAD	Comprehensive Analytical Model of Rotorcraft Aerodynamics and Dynamics code
CFD	Computational Fluid Dynamics
CFL	Courant-Friedrichs-Levy number
CPU	Central Processing Unit
DG	Discontinuous Galerkin finite element method
MBD	Multi-Body Dynamics
MTMG	MultiTime MultiGrid convergence acceleration algorithm
STMG	Time-Serial MultiGrid algorithm
OLS	Operational Loads Survey rotor
TRAC	TiltRotor Aeroacoustic Code



Symbols

D	rotor diameter
h_c	mesh width outside vortex core
h_f	mesh width in vortex core
k	number of periods
n	number of elements in vortex core
n_c	number of multigrid cycles to converge three orders
N_{4D}	number of space-time grid elements
N_A	number of grid adaptations
ψ	azimuth angle measured from tail rotor
r	flop rate
T	time period
T_{MTMG}	computing time for the MTMG algorithm
T_{STMG}	computing time for the STMG algorithm
W	number of floating point operations per element per cycle

1 Introduction

1.1 Aeroelastic response problems

Recently there has been considerable interest in The Netherlands in applications of small unmanned helicopters. To obtain good quality video images it is required to predict the vibrational modes of the unmanned helicopter for a wide maneuver envelope.

For the quantitative resolution of the aeroelastic response problem of a rotor/hub/fuselage system resulting in vibrations, it is required that an accurate aerodynamics model is coupled with a detailed elastomechanical model. In Figure 1 a conceptual description of the coupled model of rotor blade/hub/fuselage system is presented, showing the interactions between the different models for the aerodynamics, blade dynamics, trim, and the dynamics of the hub/fuselage. The elastomechanical model shown in this figure contains the various components of the rotor system, such as swashplates, pitch links, flex beams, hinges, etc. These components should be modeled in sufficient detail to enable the accurate prediction of its dynamic behaviour and associated loads. The stability of the rotorcraft system is extremely sensitive to the modeling of the damping properties (see for example Kunz (Ref. 9)). As an example, Figure 2 shows the different components of the XV-15 tilt rotor, as taken from Ghiringhelli et al. (Ref. 7). The multi-body model of the interactions between these components is shown in Figure 3, taken from Bottasso et al. (Ref. 3). It is important to realise that general purpose multibody dynamics (MBD) codes supply large modeling flexibility, and modeling details can be added easily (see Bauchau et al. (Ref. 1) for several rotorcraft applications of MBD). Unfortunately, this approach has not yet gained acceptance in the rotorcraft community. In comprehensive rotor codes the modal reduction approach is used, which requires new software developments for each new mechanical model, see for instance Kunz and Jones (Ref. 8), who modify CAMRAD to model the intricate Apache rotor system.

The importance of the accurate prediction of the blade motions under aerodynamic and structural loading has been stressed by, among others, Burley et al. (Ref. 4) in the context of the TRAC program. The blade loads, and hence the vibrational loads on the fuselage, are extremely sensitive to the elastic motions of the blades. As found by Milgram et al. (Ref. 11) and Yeo et al. (Ref. 20), comprehensive rotor codes are not capable to supply the higher harmonics of the blade loads which are needed for vibrational analysis, even for isolated rotors. Lyle et al. (Ref. 10) were surprised of the good correlation between experiment and simulation for the lower harmonics, and cautioned against extrapolation of the results to other flight conditions. As shown by Boelens et al. (Ref. 2) by the simulation of the flow about the rigid blades of the Operational Loads Survey rotor in forward flight, aerodynamic tools based on first principles of flow physics are capable of capturing

blade-vortex interaction (BVI) events which are responsible for the higher harmonics. Hence, the integrated modeling of detailed mechanical dynamics and first principles based aerodynamics is essential for vibrational analysis.

Compared to monodisciplinary simulations, computing times for the coupled simulation increase significantly, because of the disparate time scales of the problem. For helicopter simulations, the ratio of the maximum frequency of the flow physics, the BVI events, and the minimum frequency, the blade passing frequency, is in the order of hundreds. The structural dynamics reacts on the same time scale as the BVI events, whereas a trimmed solution can only be verified after the simulation of a complete revolution. Hence, a simulation of a trimmed rotor configuration including blade deformation takes a large number of revolutions.

The large number of revolutions required for coupled simulations has prompted the development of so-called weakly coupled aeroelastic simulations, where the elastomechanical model and trimming procedure are computed using standard comprehensive rotor codes based on mixed potential and lifting line models. The forces from the relatively simple aerodynamics of the rotor codes are corrected by the Computational Fluid Dynamics (CFD) results, and the blade pitch and blade deformations from the rotor code are passed to the CFD grid system. See Pahlke et al. (Ref. 12) and Servera et al. (Ref. 14) for an overview of this method. Since the rotor trim and blade deformations still depend on two-dimensional aerodynamical models, this will result in a degradation of the accuracy compared to using the 3D CFD data directly. For instance, Boelens et al. (Ref. 2) found that it is essential to trim the rotor based on the CFD results, and not on the aerodynamic models used in comprehensive rotor codes. Hence, a *strong* coupling of the elastomechanical model and trim procedure with the CFD results is preferred, where the different models interact directly.

Combination of the accuracy requirements with the system requirements of the coupled models shows that it is of the utmost importance that the computing times of the computationally most intensive part, the aerodynamic computations, are reduced significantly. This is the subject of the current report. A new solution algorithm, of which the first ideas were introduced in Van der Ven et al. (Ref. 17), will be introduced and demonstrated on the simulation of a rotor in forward flight.

1.2 Outline

The outline of the report is as follows. In Chapter 2 the solution algorithm will be presented. In Section 3 the algorithm is applied to the simulation of the Operational Loads Survey Rotor in forward flight, as yet without elasto-mechanical coupling. This simulation is meant to demonstrate the feasibility of the new solution algorithm, and an extensive discussion of the computational



complexity of the algorithm is presented. Finally, in Chapter 4 conclusions will be drawn on the affordability of forward flight simulations.



2 Multitime multigrid algorithm

In this chapter the multitime multigrid (MTMG) algorithm of Van der Ven et al. (Ref. 17) for solving time-periodic problems is described and its application to rotor flow is discussed.

2.1 Basic idea

The basic idea of the MTMG solution algorithm is that a time-periodic problem can be considered a steady problem in the sense that after one time period the next period shows the same flow phenomena, as exposed in more detail in Van der Ven et al. (Ref. 17). This is formalised by solving the time-dependent flow equations simultaneously in both space and time for the complete period of the problem. This is contrary to the usual time-serial approach, where one proceeds time step after time step on spatial grids. Now the time-dependent equations are solved on a four-dimensional space-time grid which contains all time levels in a period.

The solution approach of the four-dimensional equations is the same as for three-dimensional equations: a pseudo-time is introduced and the solution is marched to steady-state in pseudo-time by a four-dimensional multigrid algorithm. This approach is feasible since the time-dependent compressible Euler equations are hyperbolic in both space and time, hence the temporal direction can be treated like the spatial directions.

It is important to realise that the proposed algorithm is a convergence acceleration algorithm for time-dependent equations. The discretization scheme is not modified, hence its accuracy properties are retained.

2.2 Benefits

Apart from generating a periodic solution by construction, the main advantage of the solution algorithm lies in the fact that it transforms a time-dependent (*dynamic*) problem into a steady-state (*static*) problem. This has several advantages:

- as long as the solution process converges, the final solution is independent of the solution process. The underlying discretised equations are unmodified, and, moreover, there is no problem with the possible accumulation of numerical errors from preceding time steps;
- local grid refinement can be extended to the time dimension. Since there is no time direction in the solution algorithm, interpolation or the order of time steps in the case of hanging nodes are no issue;
- combining local grid refinement and parallel processing does not lead to dynamic load balancing problems. Since the local grid refinement no longer needs to be applied at each time step, the number of grid adaptations reduces significantly to about five times per simulation,

which is the usual number for steady-state simulations. Hence the parallel efficiency on a massively parallel processors (MPP) machine is not hindered by dynamic load balancing issues. Because of the grid sizes of four-dimensional grids it is expected that the MTMG algorithm easily scales to thousands of processors;

- time-accurate coupling with other physics models is straightforward.

For the strongly coupled aeroelastic simulation of a trimmed rotor/hub/fuselage system all these benefits help to decrease the computational complexity of the simulation.

Conventionally, the solution procedure for the aeroelastic simulation is as shown in Figure 4, based on the implicit/implicit staggered scheme of Wagner et al. (Ref. 19) and Piperno et al. (Ref. 13). After each period, the thrust and moments can be computed and used to trim the rotor, after which a new period is simulated. If grid adaptation were applied, dynamic load balancing problems would occur, effectively destroying any existing efficiency in other parts of the aerodynamics model than the adaptation algorithm.

In the MTMG approach all simulation data is available at all time steps, and the trust and moments are readily available to trim the rotor. Moreover, a modification in the pitch schedule will require only a small number of pseudo-time iterations for the flow solution to conform to the new schedule. Another consequence of having the data available at all time steps is that the coupling between the aerodynamics and mechanics modules can be made genuinely implicit, without the need of predictor-corrector mechanisms.

Since local grid refinement will not lead to dynamic load balancing issues in the MTMG approach, local grid refinement can be applied to decrease the required grid size (see Section 3.6 for more details). The coupling procedure for the aeroelastic simulation using the MTMG approach, including trim and grid adaptation, is shown in Figure 5.

3 Rotorcraft simulation

The simulation described below demonstrates the feasibility of the MTMG solution algorithm. The flow solver to which the solution algorithm is applied, is based on a discontinuous Galerkin (DG) finite element discretization of the unsteady compressible Euler equations (Ref. 16, 18). For the current report the most important feature of the DG method is its capability to compute accurately on locally refined meshes with hanging nodes (see Figure 8 for an example of such a grid). Note that the multitime multigrid algorithm is a solution technique which does not change the equations to be solved. Hence, the accuracy of the DG method as demonstrated in Boelens et al (Ref. 2) is unaffected.

3.1 Operational Loads Survey helicopter rotor simulation

The simulation of the Operational Loads Survey (OLS) rotor in forward flight has been repeated. This is the simulation of two rotor blades with a tip Mach number of 0.664, an advance ratio of 0.164. For details see Boelens et al. (Ref. 2). The pitch and flap schedule chosen for this test case corresponds to the schedule of (Ref. 15):

$$\theta = 6.14 + 0.9 \cos \psi - 1.39 \sin \psi, \quad \beta = 2.4 - 1.0 \cos \psi,$$

(in degrees), where ψ is the azimuth angle, measured from the tail rotor, θ the pitch angle, and β the flap angle. The pitch schedule corresponds to the trimmed pitch schedule of the experiment, but as found in Boelens et al. the schedule does not lead to a trimmed rotor for the Euler equations.

An initial three-dimensional mesh containing 244,224 elements has been used to generate a four dimensional mesh using the pitch and flap schedule for the blade movement. A time step equivalent to a rotor rotation of ten degrees has been used. Even though the simulation is periodic with a period equal to half a revolution, a complete revolution is contained in the space-time grid. To be able to simulate only half a revolution the original space grid should have a two-fold rotation symmetry, which was not the case. The fourdimensional mesh contains 8,792,064 cells.

3.2 Space-Time grid adaptation

The grid adaptation algorithm is as follows. The space adaptation is not modified with respect to the time serial simulations of (Ref. 2): the vorticity sensor combined with the mesh width sensor is used to generate a uniform mesh in the vortex region. As in the previous simulations the target mesh width is $0.005D$, where D is the rotor diameter, so cells are refined as soon as the mesh width in a certain direction is greater than $0.01D$ (see Section 3.6 for a discussion on the required resolution in vortex regions). The time sensor in principle refines cells in time whenever the space sensor is active, *and* the physical CFL number (the CFL number based on the physical time step

	Run 1 ^b of (Ref. 2)	MTMG initial grid	MTMG final grid
$C_Z(\times 10^3)$	4.999	5.60	5.23
$C_{M_X}(\times 10^3)$	0.117	0.132	0.148
$C_{M_Y}(\times 10^3)$	0.499	0.541	0.494

Table 3 Period-averaged thrust and moments

in stead of the local psuedo time step) is greater than one. In this way the grid converges to a grid where the physical CFL number is about one in the flow regions of interest, which is essential for vortex persistence.

The total simulation consisted of 1700 multitime multigrid cycles, and twelve grid adaptations were performed, of which five adapted the grid only in time.

3.3 Results

In Figure 6 the convergence history is shown for the first part of the computation, showing the Full Multigrid approach and the first two grid adaptations. The convergence rate of the MTMG solver is good, and comparable to the rate for three-dimensional simulations. Extrapolating the convergence rate, the MTMG method requires 500 multigrid cycles for the residuals to drop three orders. After each adaptation residuals drop at least two orders (not shown), and finally a decrease of three orders in the residuals has been reached. In Figure 7 the final thrust coefficient and roll and pitch moments are shown. The averaged forces are shown in Table 3. To assess the influence of the grid adaptation on the aerodynamic coefficients, the computed forces are also shown for the initial non-refined mesh. Compared to earlier time serial results of (Ref. 2) obtained using a time step of five degrees, the difference is most probably caused by the fact that the time serial results correspond to the second revolution of the computation, so the simulation had not reached a periodic state yet. This stresses the need to ascertain the periodicity of the solution obtained using the conventional time-serial algorithm. In Van der Ven et al. (Ref. 17) it was shown that convergence to a periodic solution using the time-serial algorithm can be rather slow (also see Section 3.5).

In Figures 8 and 9 the final grids and three-dimensional flow results on the final grid are shown for two time instants. The grid is shown at the cross-section $z = 0$ (the horizontal symmetry plane of the mesh when all trim parameters are zero). Clearly visible are the refined vortex regions. The grid resolution in the vortex regions is about a factor of two coarser than in (Ref. 2), but sufficiently fine to be able to compare the two methods.



The time refinements can be made visible by plotting the grid at newly generated time levels. The present postprocessing utilities of the flow solver will only show the cells present at the specified time levels. The resulting grids at time levels corresponding to $\psi = 101.25^\circ$ and $\psi = 151.25^\circ$ are shown in Figure 10. The 3D vortex structures are clearly visible. Note that a time step of 1.25 degrees was used in the later runs of (Ref. 2), so the time refinement of the current simulation has reduced the initial time step of 10 degrees in the vortex regions to the time step required for accuracy.

At each four-dimensional grid adaptation the grid size is increased by 10%; when the grid is only adapted in time the grid size increased by 5%. The final grid contains almost 25 million cells, three times the original number. Note that in the DG method there are 25 degrees of freedom per cell, five for each conservative variable. Hence the final grid size represents 625 million degrees of freedom.

In Figure 11 the time series of the differential pressure $\Delta C_p M^2$ are shown for several blade stations. A comparison is made with the initial solution and the solution on the final refined mesh. The differences between the initial and final results are most expressed at cross-section $r/R = 0.5$, where the vortex from the receding blade is more resolved on the final grid. Last but not least, Figure 12, showing the differential pressure profiles for the two blades simultaneously, demonstrates that the MTMG algorithm produces a periodic flow, that is, the same differential pressure on both blades.

These results demonstrate both convergence of the MTMG solution algorithm and its capability for vortex resolution through local grid refinement in both space and time.

3.4 Computational characteristics

The flow solver runs at an average speed of 3 Glop/s (37.5% peak) on one NEC SX-5/8B processor. With the current grid sizes it is easy to maintain this speed on more processors, and on six processors a speed of 18 Glop/s was obtained. The computational speed is $7.8 \cdot 10^{-5}$ CPU second per element per multigrid cycle, where each cycle consists of one prerelaxation and one postrelaxation. Hence one hundred pre- and postrelaxations on the final grid with 25 million cells take nine hours to complete on six processors.

The flow solver requires 1.8 kByte per cell, that is 72 Byte per unknown, since each cell contains five unknowns for the five conservative variables. The maximum memory on the NLR NEC SX-5/8B is 54.5 GByte, which implies that the maximum number of grid cells for the flow solver on the NLR NEC SX-5/8B is almost 32 million cells. The final refined mesh consumes 42 GByte main memory.

The grid adaptation algorithm requires more memory than the flow solver, since in the current implementation the data for the newly generated cells is computed first for all new cells, before the old data is removed. The final grid adaptation step consumed 53 GByte of main memory, which is almost the limit of the NLR NEC SX-5/8B. The average computing time of the scalar grid adaptation algorithm is five hours on a grid of about 15 million cells. A greater part of this computing time is spent in dynamically reallocating to larger datastructures and recomputing certain topological relations.

The combined computation time of the complete run including the twelve grid adaptations on six processors of the NLR NEC SX-5 is less than one hundred hours.

3.5 Discussion of computational complexity

In this section the computational complexity of the MTMG algorithm for the above simulation is compared with the computational complexity of the conventional algorithm applied in Boelens et al. (Ref. 2). The comparison of the computational complexity of the MTMG solution method with the conventional time integration scheme (denoted by STMG) is done in two steps. Firstly, the methods are compared on equivalent grid sizes. Secondly, the methods are compared on locally refined meshes.

The grid sizes for the two methods are called equivalent if the spatial resolutions are the same, and the number of time steps on the fourdimensional mesh for MTMG is equal to the number of time steps per period for the STMG method. If the grid sizes are equivalent, the grids have the same size in the space-time domain. Since the discretised equations are the same for both methods, the number of floating point operations per element per time step per iteration are equal. So the computing times on equivalent grids are the same for the two methods. The only difference in overall computing time is caused by the different convergence rates of the two methods. On the initial grid of 244,224 spatial elements and a time step corresponding to $\Delta\Psi = 10^\circ$ the MTMG method requires 500 multigrid cycles to converge three orders (extrapolated from the results shown in Figure 6). The STMG method requires 100 multigrid cycles per time step to converge three orders. Hence, *per period* the MTMG method is 5 times slower than the STMG method.

However, the residuals of the two methods do not measure the same quantity. The convergence to a periodic solution is not measured by the STMG residuals. Van der Ven et al. (Ref. 17) have shown that for the periodic problem of an oscillating airfoil convergence to a periodic solution is extremely slow: in five periods the residual measuring the periodicity of the solution hardly dropped one order. Extrapolating this result to the simulation of a rotor in forward flight is not straightforward, but considering the increased bandwidth of the problem, it is reasonable to assume

that the STMG method requires at least thirty periods to converge to a reasonably periodic solution. Hence, the MTMG method is $30/5 = 6$ times faster than the STMG method in obtaining a periodic solution on equivalent grids.

In Boelens et al. (Ref. 2) the adaptation strategy for the STMG method locally refined the spatial grid at each time step without coarsening the mesh. This strategy avoids grid refinement and de-refinement at each step, which is a costly process, but, since the grid refinement is effectively integrated in time, results in a uniformly refined mesh in the complete rotor disk area. The final grid size was 1.3 million elements, and the resolution was such that an overall time step equivalent with $\Delta\Psi = 1.25^\circ$ was required for accuracy. Hence, an equivalent space-time grid would contain 375 million elements. The MTMG method demonstrates the same accuracy in terms of vortex capturing on a mesh containing 25 million elements, a factor of 15 decrease in grid size. In Section 3.6 an analysis of the required grid sizes is made.

Neglected in the above comparison is the time required to obtain the final locally refined mesh. For the STMG method combined with the above adaptation strategy one period was required. This is negligible with respect to the number of periods required to obtain a periodic solution. The MTMG method, however, required twelve grid adaptations. The computing time for the MTMG method is directly proportional to the number of grid adaptations.

Summarising the above the speedup of the MTMG over the STMG method can be expressed as the ratio of the respective computing times:

$$\frac{T_{\text{STMG}}}{T_{\text{MTMG}}},$$

where

$$T_{\text{STMG}} = k \cdot n_c \cdot N_{4\text{D}} W / r,$$

$$T_{\text{MTMG}} = N_A \cdot n_c \cdot N_{4\text{D}} W / r,$$

where k is the number of periods, n_c is the number of STMG or MTMG cycles required to reduce the residuals by three orders in magnitude, $N_{4\text{D}}$ is the grid size in the space-time domain (including number of time steps per period for the STMG method), W is the flop count per element per cycle, r is the flop rate on a specific machine, and N_A is the number of grid adaptations.

By the above reasoning, $k = 30$, $n_c(\text{STMG}) = 100$, $n_c(\text{MTMG}) = 500$, $N_{4\text{D}}(\text{STMG}) = 15N_{4\text{D}}(\text{MTMG})$, $N_A = 12$, and W/r is independent of the method. Hence,

$$\frac{T_{\text{STMG}}}{T_{\text{MTMG}}} = \frac{k \cdot n_c(\text{STMG}) \cdot N_{4\text{D}}(\text{STMG})}{N_A \cdot n_c(\text{MTMG}) \cdot N_{4\text{D}}(\text{MTMG})} = \frac{30 \cdot 15}{12 \cdot 5} = 7.5.$$

It is clear from this expression that a reduction of the number of grid adaptations would enhance the speedup. The number of grid adaptations is quite large, compared to steady-state simulations. This is partly due to the fact that the computation started with a mesh with a time step of ten degrees, which is large compared to the spatial resolution of the mesh. If the computation could have started with a mesh containing only half a revolution, time steps of five degrees would have been feasible, decreasing the adaptation effort to $N_A = 6$. Nonetheless, adaptation criteria need to be improved in order to be able to reduce the number of grid adaptations to about four, one third of the number of grid adaptations of the present simulation. If these adaptation criteria are developed, the speedup would be more than 20.

3.6 Grid size estimates

In the previous section the ratio of required grid sizes for the STMG and MTMG solution methods was compared for a particular simulation. In this section, a grid size analysis will be made based on the length and time scales of a general rotor in forward flight. Let D be the rotor diameter, r be the typical core size of a vortex, and $T = 2\pi/n_b\Omega$ the periodicity of the rotor system, where n_b is the number of blades, and Ω the rotational frequency of the blades. The volume of the computational domain is proportional to D^3 , and as argued in Caradonna (Ref. 5), $r = 0.01D$. Let n be the number of grid cells required in each direction to capture the vortex. Then the mesh width h_f required in the vortex is r/n . A *uniform* mesh would contain

$$\frac{D^3}{h_f^3} = \left(\frac{D}{r}\right)^3 n^3 = 10^6 n^3$$

grid points. With $n = 10$ we obtain the grid size mentioned by Caradonna (Ref. 5).

Local grid refinement can alleviate this excessive resolution requirement, by ensuring the required resolution h_f only in the vortex regions. The vortex length is proportional to D , so the volume of the vortex region is Dr^2 , which is only 0.01% of the computational domain. Outside these regions a resolution with mesh width $h_c = D/100$ will suffice. For steady state simulations for a rotor in hover the grid size is now

$$\frac{Dr^2}{h_f^3} + \frac{D^3 - Dr^2}{h_c^3} \approx \frac{D}{r} n^3 + 10^6 = 100n^3 + 10^6.$$

Clearly, the required number of grid points is not dominated by the resolution in the vortex region, and a grid with a million grid points suffices, demonstrating the strength of local grid refinement.

For time dependent problems dynamic load balancing issues will inhibit the use of local grid refinement and derefinement at each time step, and the spatial resolution for the rotor in hover



cannot be maintained. As described in Section 3.5, Boelens et al. (Ref. 2) applied an adaptation strategy for the STMG method which effectively refined the whole rotor disk with volume $0.1D^3$, assuming that the rotor plane is tilted over an angle of five degrees. Since the time step Δt required for accuracy is proportional to the smallest mesh width, $\Delta t \sim h_f$. So the required number of grid points in the space-time domain for the STMG algorithm is

$$N_{4D}(\text{STMG}) \sim \left(\frac{0.1D^3}{h_f^3} + \frac{D^2(D-r)}{h_c^3} \right) \frac{T}{h_f} \approx \left(0.1n^3 \left(\frac{D}{r} \right)^3 + 10^6 \right) n \frac{T}{r}. \quad (1)$$

In the MTMG approach we do not have any load balancing issues and we can adapt the grid when and where a vortex is present, hence the spatial resolution for the rotor in hover is restored. The small time step $\Delta t = h_f$ is only needed in the vortex regions, and a time step $\Delta t = h_c$ suffices in the other regions. So the space-time grid size for the MTMG algorithm is

$$N_{4D}(\text{MTMG}) \sim \frac{Dr^2}{h_f^3} \frac{T}{h_f} + \frac{D(D^2-r^2)}{h_c^3} \frac{T}{h_c} \approx \left(n^4 \frac{D}{r} + 10^8 \frac{r}{D} \right) \frac{T}{r}. \quad (2)$$

Combining (1) and (2), the ratio of the optimal grid sizes for the two approaches is

$$\begin{aligned} \frac{N_{4D}(\text{STMG})}{N_{4D}(\text{MTMG})} &= 0.1 \left(\frac{D}{r} \right)^2 \frac{1 + 10^7 n^{-3} \left(\frac{r}{D} \right)^3}{1 + 10^8 n^{-4} \left(\frac{r}{D} \right)^2} \\ &= 1000 \frac{1 + n^{-3} 10^2}{1 + n^{-4} 10^4}. \end{aligned}$$

For $n = 10$ the ratio of the required grid sizes is 500. Since the DG method has two degrees of freedom per cell in each direction, for DG $n = 5$ is sufficient to capture the vortex. For $n = 5$ the ratio of the required grid sizes is 64. This is more than attained in the simulation in Section 3.5, since both simulations did not achieve the required resolution of $r/5$ in the vortex region. The theoretical analysis stresses and confirms that a significant gain in grid size can be obtained by the MTMG algorithm combined with local grid refinement.

4 Conclusions

For the vibrational analysis of a rotor/hub/fuselage system it is essential that

- the aerodynamics model is *strongly* coupled to the elasto-mechanical models,
- the aerodynamics model is based on first principles,
- the rotor system is trimmed on the basis of the CFD results.

Straightforward implementation of these points of departure would yield a helicopter vibrations analysis system which requires prohibitively large computing times, due to disparate time scales and high resolution requirements. To overcome the apparent computational complexity of the system, a new fourdimensional solution method has been presented. The solution method decreases both the numerical complexity of the coupled system, and its computational complexity, by turning a dynamic problem into a static problem. Local grid refinement can be used to decrease the CFD grid size, without jeopardising the parallel efficiency of the method.

The solution method has been applied to the simulation of the flow around a rotor in forward flight, combined with local grid refinement in both space and time. The method demonstrated good vortex capturing capabilities on a space-time grid which was a factor 15 smaller than the equivalent spatial grid of earlier conventional simulations. The overall computational complexity has been shown to be reduced by a factor of 7.5 compared to the conventional solution method. It is expected that when better grid adaptation procedures will be developed, this factor may increase to more than sixty.

The computational complexity of the most compute intensive part of the coupled system for aeroelastic response problems has been reduced significantly. A clear development path has been identified to reach the ultimate goal of affordable and accurate vibrational analysis of rotor/hub/fuselage systems.

5 References

1. O.A. Bauchau, C.L. Bottasso, and Y.G. Nikishkov. Modeling rotorcraft dynamics with finite element multibody procedures. *Math. Comput. Modeling*, 33:1113–1137, 2001.
2. O.J. Boelens, H. van der Ven, B. Oskam, and A.A. Hassan. Boundary conforming discontinuous Galerkin finite element approach for rotorcraft simulations. *J. of Aircraft*, 39 (5):776–785, sep-oct 2002. Also NLR-TP-2002-460.
3. C.L. Bottasso, L. Trainelli, P. Abdel-Nour, and G. Labò. Tilt rotor analysis and design using finite-element multibody procedures. In *Proceedings of the 28th European Rotorcraft Forum, September 17-20, 2002, Bristol, 2002*.
4. C.L. Burley, T.F. Brooks, B.D. Charles, and M. McCluer. Tiltrotor aeroacoustic code (TRAC) prediction assessment and initial comparison with TRAM test data. In *Proceedings of the 25th European Rotorcraft Forum, September 14-16, 1999, Rome, 1999*.
5. F.X. Caradonna. Development and challenges in rotorcraft aerodynamics. *AIAA*, 2000-0109, 2000.
6. P. Wilders et al., editor. *International Parallel CFD 2001 Conference*. North-Holland, Elsevier, May 21-23 2002.
7. G.L. Ghiringhelli, P. Masarati, P. Mantegazza, and M.W. Nixon. Multi-body analysis of the 1/5 scale wind tunnel model of the v-22 tiltrotor. In *Proceedings of the American Helicopter Society 55th Annual Forum, May 25-27, 1999, Montreal, 1999*.
8. H.E. Jones and D.L. Kunz. Comprehensive modeling of the Apache with CAMRAD II. In *Proceedings of the American Helicopter Society Hampton Roads Chapter, Structure Specialists' Meeting, Williamsburg, October 30-November 1, 2001, 2001*.
9. D.L. Kunz. Nonlinear analysis of helicopter limit cycle oscillations. In *Proceedings of the American Helicopter Society Aeromechanics Specialists Meeting, Atlanta, November 13-14, 2000, 2000*.
10. K.H. Lyle, C.L. Burley, and D.S. Prichard. A comparison of measured and predicted XV-15 tiltrotor surface acoustic pressures. In *Proceedings of the AHS Technical Specialists' Meeting for Rotorcraft Acoustics and Aerodynamics, October 28-30, 1997, Williamsburg, 1997*.
11. J. Milgram and I. Chopra. Helicopter vibration reduction with trailing edge flaps. In *Proceedings of the 36th AIAA/ASME/ASCE/AHS/ASC Structures, Structural Dynamics, and Material Conference, April 10-12, 1995, New Orleans, 1995*.
12. K. Pahlke and B. van der Wall. Progress in weak fluid-structure-coupling for multibladed rotors in high speed forward flight. In *Proceedings of the 28th European Rotorcraft Forum, September 17-20, 2002, Bristol, 2002*.

13. S. Piperno, C. Farhat, and B. Larrouturou. Partitioned procedures for the transient solution of coupled aeroelastic problems, Part I: Model problem, theory and two-dimensional application. *Comput. Meth. Appl. Mech. Engrg.*, 24:79–112, 1995.
14. G. Servera, P. Beaumier, and M. Costes. A weak coupling method between the dynamics code HOST and the 3D unsteady Euler code WAVES. In *Proceedings of the 26th European Rotorcraft Forum, September 26-29, 2000, The Hague, 2000*.
15. R.C. Strawn, J. Ahmad, and E.P.N. Duque. Rotorcraft aeroacoustics computations with overset-grid CFD methods. *paper presented at the 54th American Helicopter Society Annual Forum, Washington DC, May 22-24 1998*.
16. J.J.W. van der Vegt and H. van der Ven. Space-time discontinuous Galerkin finite element method with dynamic grid motion for inviscid compressible flows. Part I. General formulation. *J. Comput. Phys.*, 182:546–585, 2002. Also NLR-TP-2001-604.
17. H. van der Ven, O.J. Boelens, and B. Oskam. Multitime multigrid convergence acceleration for periodic problems with future applications to rotor simulations. In (*Ref. 6*), pages 355–363, 2002. Also NLR-Tp-2001-363.
18. H. van der Ven and J.J.W. van der Vegt. Space-time discontinuous Galerkin finite element method with dynamic grid motion for inviscid compressible flows. Part II. Efficient flux quadrature. *Comput. Meth. Appl. Mech. Engrg.*, 191:4747–4780, 2002. Also NLR-TP-2001-605.
19. S. Wagner, A.R.M. Altmikus, and H. Pomin. Coupled numerical simulation of aerodynamics and rotor dynamics of a helicopter in forward flight. In *Proceedings of the Fifth World Congress on Computational Mechanics, Vienna, Austria, July 7th - 12th, 2002*, <http://wccm.tuwien.ac.at/>, 2002.
20. H. Yeo and P.M. Shinoda. Investigation of rotor loads and vibration at transition speed. In *Proceedings of the American Helicopter Society 58th Annual Forum, June 11-13, 2002, Montreal, 2002*.

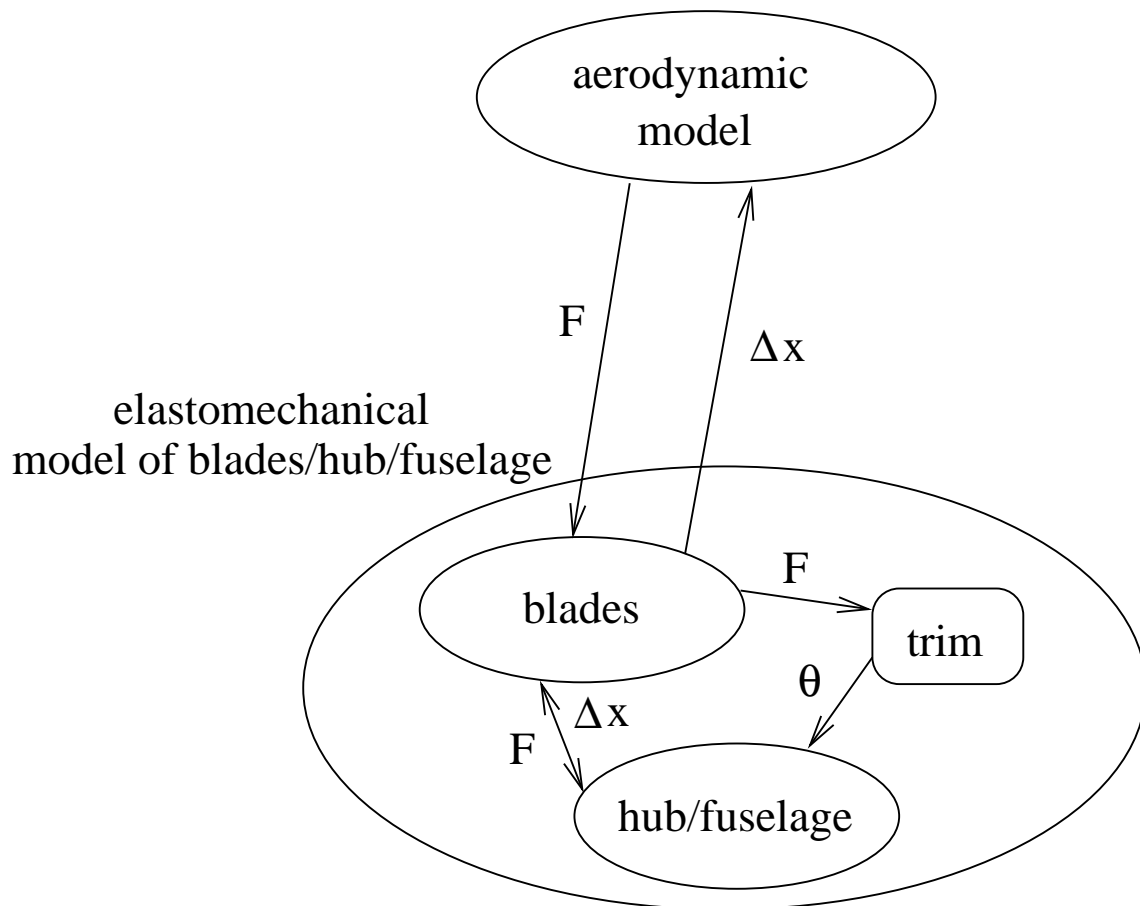


Fig. 1 Coupled models and their interactions for the aeroelastic response problem of the rotor/hub/fuselage system. The separate components of the mechanics model of the rotor system are the blades, which interact both with the aerodynamics and the hub/fuselage system, and the hub/fuselage system, which interacts with the blades. Interactions are either forces, denoted by F , or displacements, Δx . Based on the forces on the blades, the rotor is trimmed to a new schedule, denoted by θ , which is input for the hub/fuselage system. An example of the elastomechanical model of hub and fuselage is shown in Figure 3.

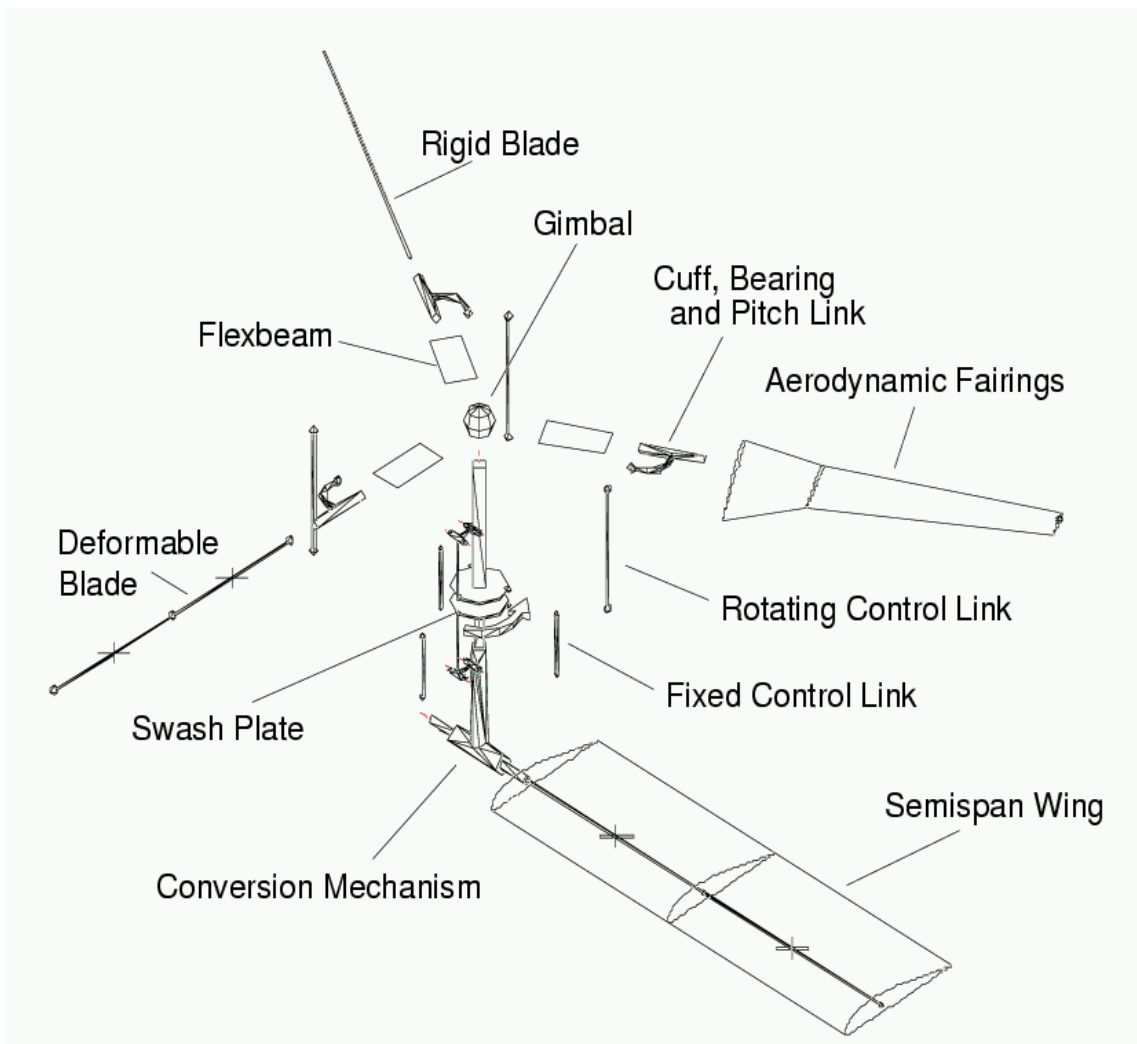


Fig. 2 Schematised representation of the xv15 tiltrotor system, showing the wing, pylon, hub, and blades (taken from Ghiringhelli et al. (Ref. 7))

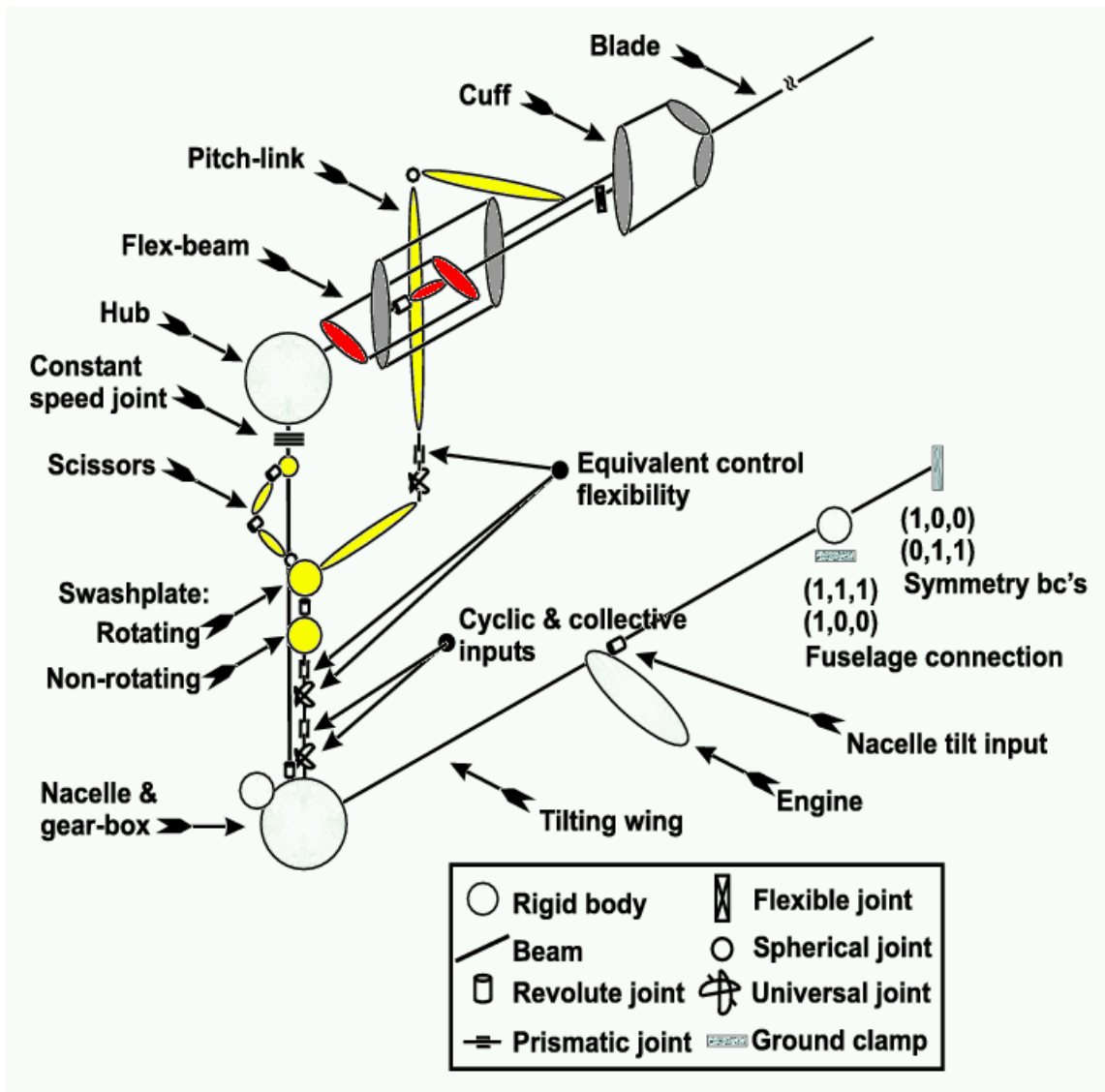


Fig. 3 Topological representation of the tilt rotor multibody model (taken from Bottasso et al. (Ref. 3))

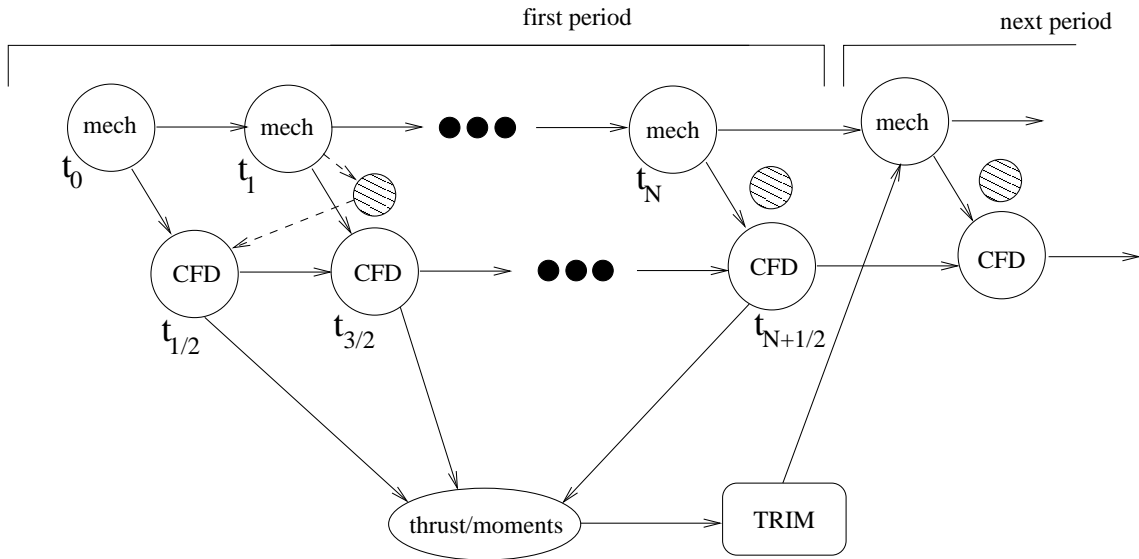


Fig. 4 Conventional time serial coupling procedure for the aeroelastic modeling of the rotor/hub/fuselage system, including trim. Shown is the implicit/implicit staggered scheme of Wagner et al. (Ref. 19). After each revolution the thrust and moments are collected and used to trim the rotor system, after which the mechanics/CFD iterations are restarted.

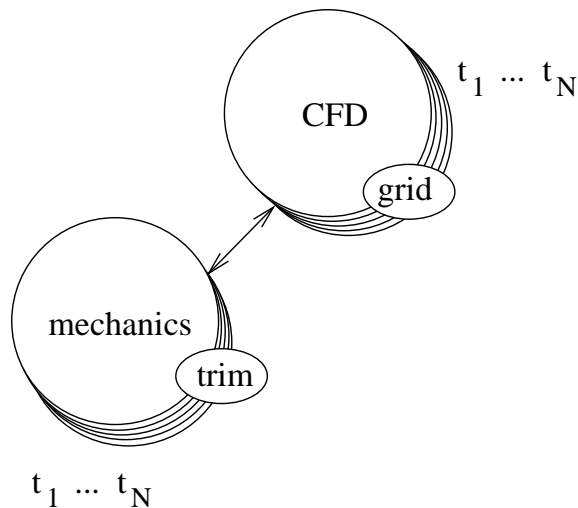


Fig. 5 Coupling procedure for the aeroelastic modeling of the rotor/hub/fuselage system, including trim and grid adaptation, using the MTMG solution algorithm.

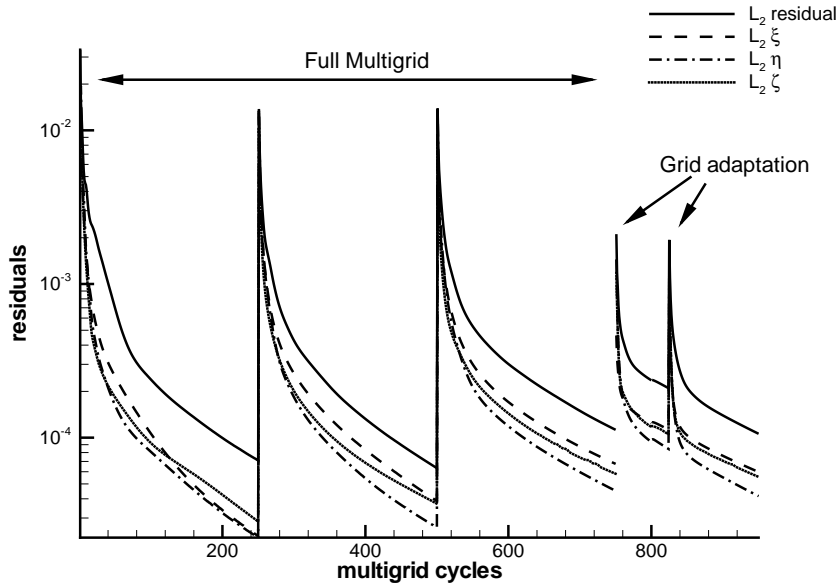


Fig. 6 First part of the convergence history, showing the full multigrid cycles on the initial grid, and the first two grid adaptations

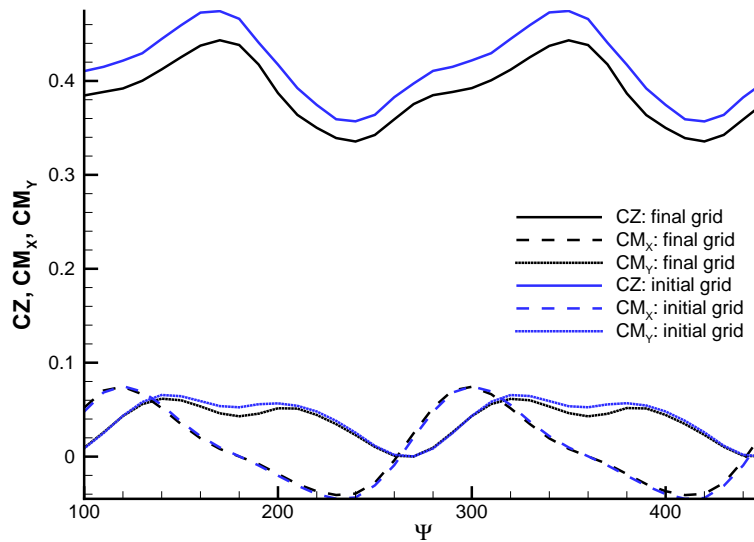


Fig. 7 Thrust and momentum coefficients for initial and final grids

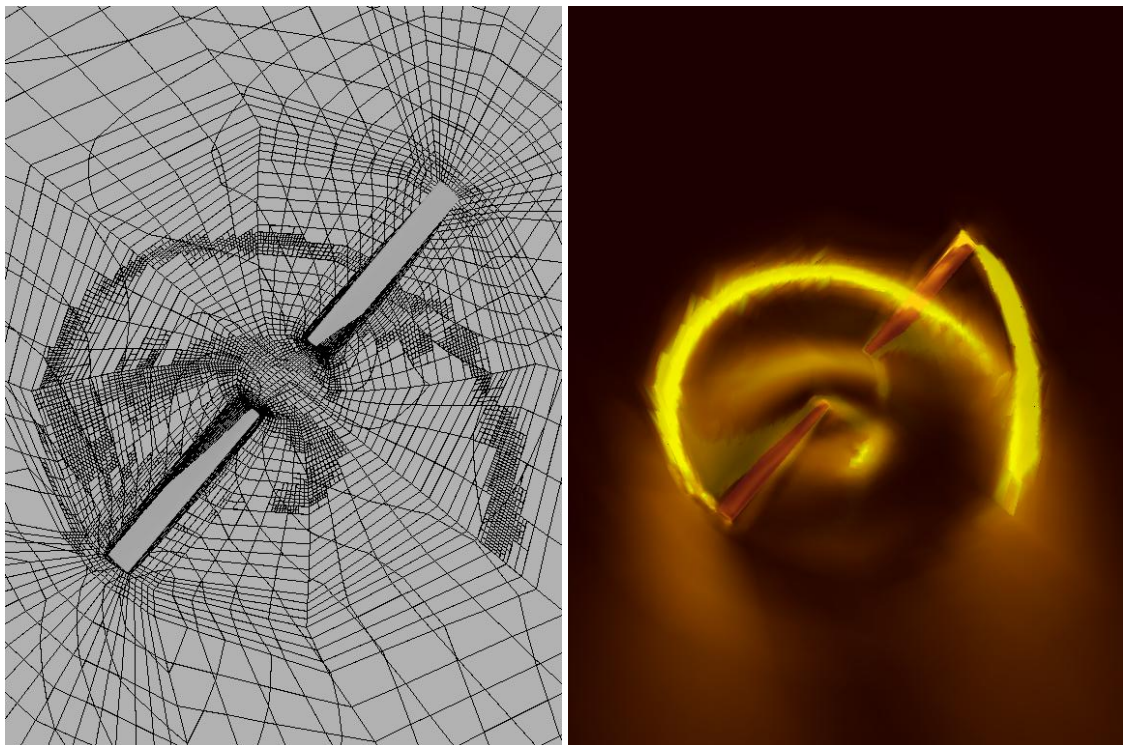


Fig. 8 Grid cross-section at $z = 0$ and vorticity levels on final grid at $\psi = 140^\circ$. The tip vortex of the blade in the upper corner lies above the $z = 0$ plane. Flow is coming from the top of the page.

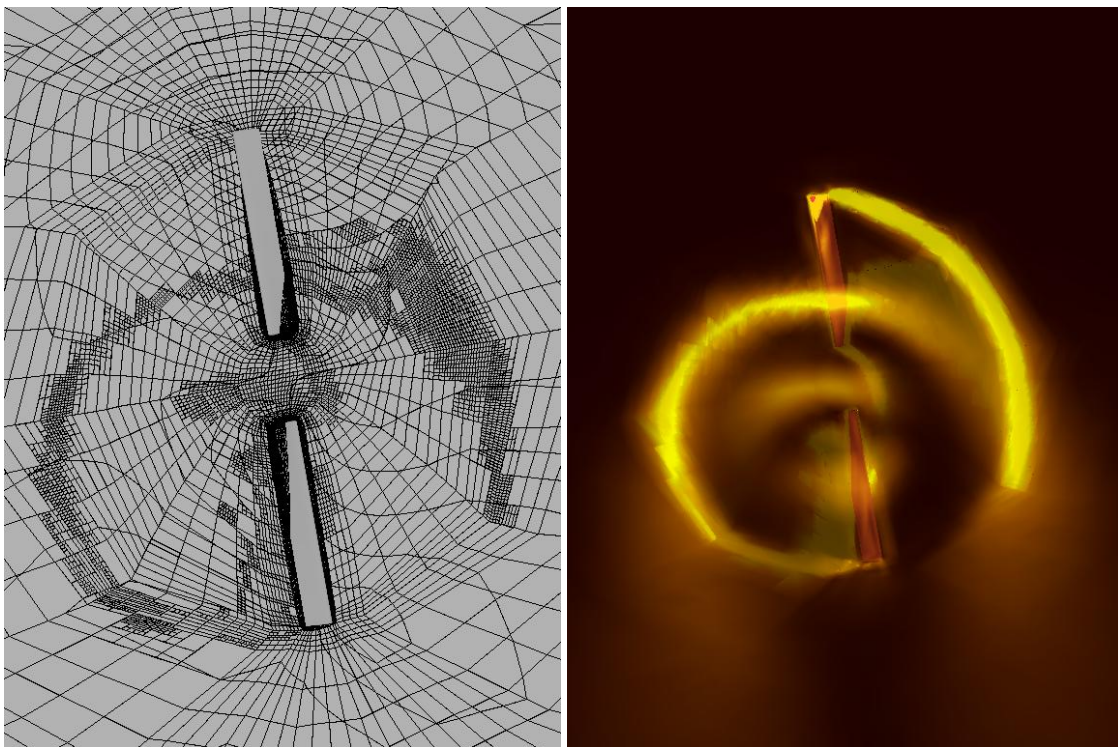


Fig. 9 Grid cross-section at $z = 0$ and vorticity levels on final grid at $\psi = 190^\circ$. The tip vortex of the upper blade lies above the $z = 0$ plane. Flow is coming from the top of the page.

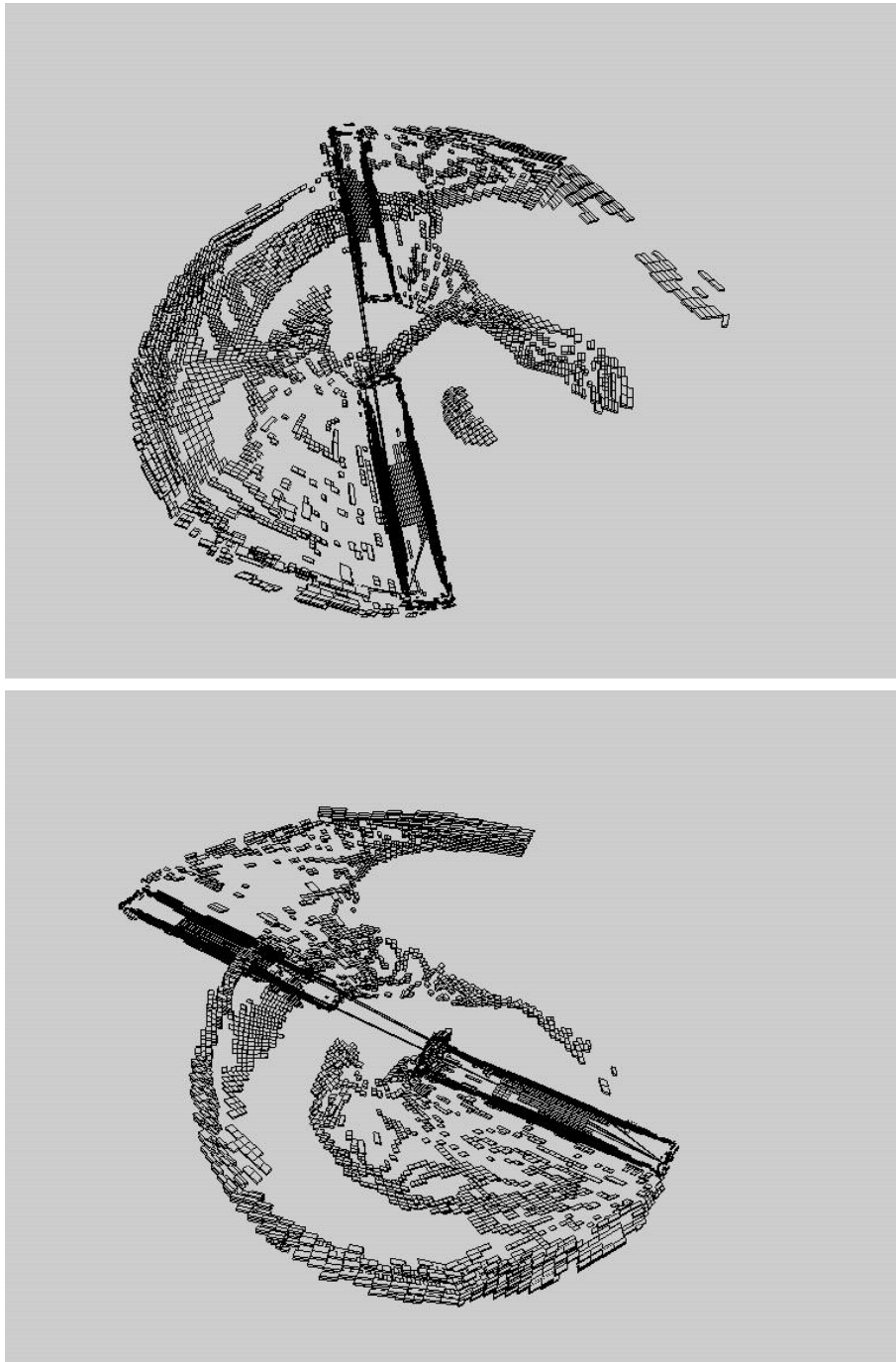


Fig. 10 Full space grids of final grid at $\psi = 101.25^\circ$ and $\psi = 151.25^\circ$. Flow is coming from the left.

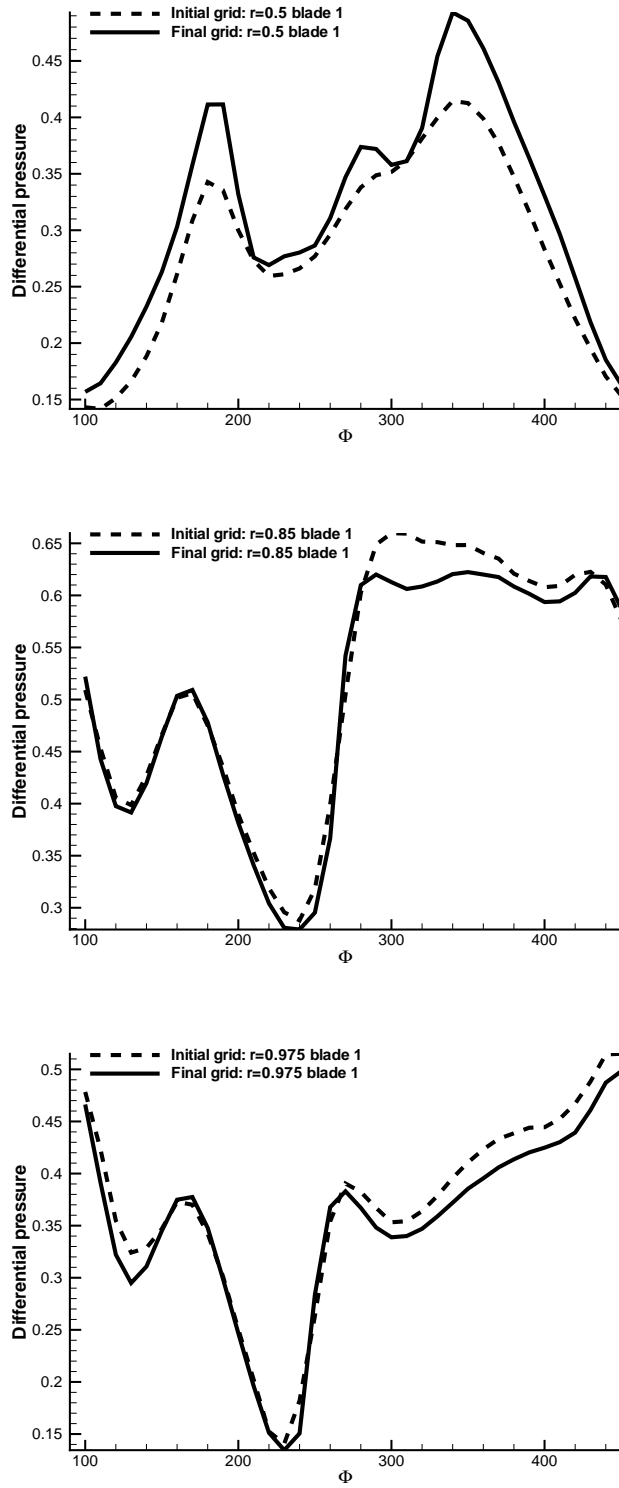


Fig. 11 Differential pressures at $r/R = 0.5$, $r/R = 0.85$, $r/R = 0.975$.

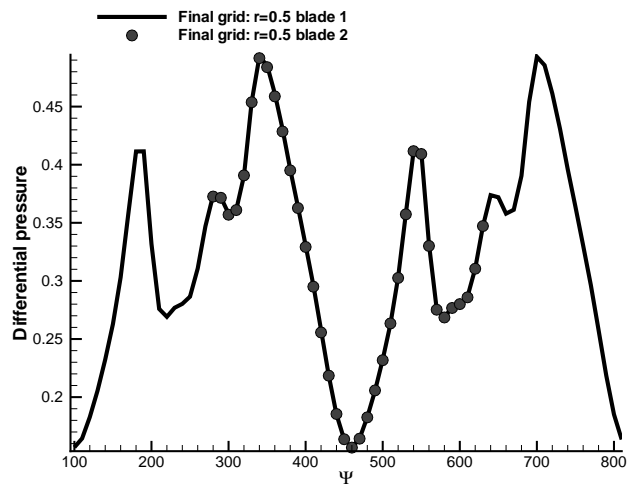


Fig. 12 Differential pressure at $r/R = 0.5$, demonstrating the periodicity of the solution by showing the differential pressures on both blades.